Elucidating Ionic Liquid Environments That Affect the Morphology of TiO2 Nanocrystals: A DFT plus D Study

ARTICLE *in* THE JOURNAL OF PHYSICAL CHEMISTRY C · OCTOBER 2014

Impact Factor: 4.77 · DOI: 10.1021/jp503891s

8 AUTHORS, INCLUDING:

Jiaqi Fu
Peking University
7 PUBLICATIONS **46** CITATIONS
SEE PROFILE

Lianjie Zhu
Tianjin University of Technology
25 PUBLICATIONS **308** CITATIONS
SEE PROFILE

Xiaochuan Duan
Xiamen University
53 PUBLICATIONS **1,348** CITATIONS
SEE PROFILE

Wenjun Zheng
Nankai University
112 PUBLICATIONS **2,295** CITATIONS
SEE PROFILE

THE JOURNAL OF PHYSICAL CHEMISTRY C

Article

pubs.acs.org/JPCC

Elucidating Ionic Liquid Environments That Affect the Morphology of TiO_2 Nanocrystals: A DFT+*D* Study

Kezhen Qi,[†,‡,#] Di Li,[†,‡] Jiaqi Fu,[∥] Lianjie Zhu,[⊥] Xiaochuan Duan,[†,‡] Qing Qin,[†,‡] Guichang Wang,*[,§] and Wenjun Zheng*[,†,‡]

[†]Department of Materials Chemistry, Key Laboratory of Advanced Energy Materials Chemistry (MOE), TKL of Metal and Molecule-Based Materials Chemistry, College of Chemistry, Nankai University, Tianjin 300071, People's Republic of China

[‡]Collaborative Innovation Center of Chemical Science and Engineering (Tianjin), Tianjin 300072, People's Republic of China

[§]Department of Materials Chemistry, College of Chemistry, Nankai University, Tianjin 300071, People's Republic of China

[∥]College of Chemistry and Molecular Engineering, Peking University, Beijing 100871, People's Republic of China

[⊥]School of Chemistry and Chemical Engineering, Tianjin University of Technology, Tianjin 300191, People's Republic of China

[#]College of Chemistry and Life Science, Shenyang Normal University, Shenyang 110034, People's Republic of China

Supporting Information

ABSTRACT: Using ionic liquids as controlling agents is known to effectively affect the morphologies of TiO_2 crystals. To obtain a profound understanding of this observation, density functional theory calculations with inclusion of Grimme treatment of the dispersion forces (DFT+*D*) have been performed to study a typical ionic liquid 1-ethyl-3-methylimidazolium bromide ([Emim]Br) adsorption on the low-index TiO_2 facets, and the equilibrium crystal shape of TiO_2 has been predicted using Wulff's rule. [Emim]Br is found to adsorb most strongly on (110) for rutile and (100) for anatase. The gap of surface energy shows an obvious increase after [Emim]Br adsorption, especially, between (101) and (001) for anatase and also between (110) and (001) for rutile. This gap variation results in increasing the (100) facet exposure of anatase, and an increase in the length-to-diameter ratio of rutile nanocrystals, which is verified by our experiments. This study is meaningful to gain further understanding of how ionic liquids achieve shape-controlled nanocrystals synthesis by turning surface chemistry, which will push a valuable step toward the ultimate goal, controlling synthesis of inorganic nanomaterials.

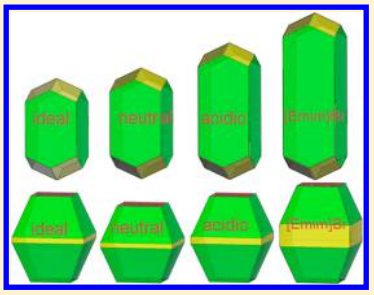

1. INTRODUCTION

Titanium dioxide (TiO_2), as an important functional material, has aroused enormous interest due to its potential applications in various fields, especially, solar cells, gas sensors, and photocatalysts.[1] These applications result from its unique physical and chemical properties, which depend not only on the phase and the size but also on the shape and the exposed facets.[2] For instance, Joo et al. demonstrated that rutile TiO_2 nanorods exhibit superior photocatalytic inactivation of *Escherichia coli* than that of Degussa P25.[3] Murakami et al. showed that the activity of acetaldehyde decomposition is higher in sharp anatase TiO_2 nanocrystals dominated by the (101) facet.[4] Obviously, controlling the shape of crystals is of key importance in the fabrication of materials with desired properties. However, the morphology control is still a great challenge in the field of nanotechnology because the small changes of growth environment can have spectacular effects on the morphologies of crystals.[5]

Recently, ionic liquids (ILs) have become a kind of fascinating reaction medium component for the synthesis of inorganic nanomaterials, because they offer the potential for morphology control that is not possible from other synthetic methods.[6] ILs can form highly ordered structures on the growing crystal facets through their wealth of noncovalent interactions (including electrostatic, hydrogen bond, and $\pi-\pi$ stacking, etc.),[7] and this modification of surface chemistry and energetics of primary nanocrystals are both important factors for affecting the shape of nanocrystals. Thus, ILs are expected to offer an efficient conditioning medium for the shape-controlled synthesis of nanocrystals. To date, various shapes of TiO_2 nanocrystals have been prepared via IL-involved processes, such as, nanorods,[8] nano-/microspheres,[9] nanocuboids and nanosheets,[10] nanobipyramids,[11] and nanotubes.[12] Although these studies have provided some insight into the factors that control the crystal growth and ultimately determine the morphologies of crystals, the shape evolution mechanisms are mostly given based on some experimental speculation. Thus, a theoretical understanding of the relationship between the growth environment and the resulting crystal morphology is urgently called for.

Density functional theory (DFT) calculation, as an effective tool in exploration of surface chemistry, has been widely used to investigate the underlying mechanism on how the growth environments affect the crystal morphologies.[13] For instance,

Received: April 21, 2014
Revised: September 6, 2014
Published: September 9, 2014

dx.doi.org/10.1021/jp503891s | *J. Phys. Chem. C* 2014, 118, 23320−23327

Yang et al. through DFT calculation predicted that using the fluorine ion as the controlling agent to turn the surface energies can successfully synthesize the anatase TiO_2 with high (001) exposure.[14] Barnard et al. had done a series of investigations on the shape transitions of TiO_2 nanocrystals using DFT calculation.[15] However, most of these studies are mainly based on standard DFT calculations, without an explicit account for sizable van der Waals interactions that can actually play a significant role due to the presence of large and highly polarizable polyaromatic rings.[16] In recent years, the semiempirical Grimme extension of the standard DFT method (DFT+*D*), an effective way of incorporating dispersion interaction, has demonstrated its ability to provide reliable modeling of molecular geometries and better description of the interaction between the organic molecules and metal oxide substrates.[17] However, as we known, almost no attempt has been made yet to analyze adsorption of IL systems.

In this work, we use DFT+*D* methods to explore the properties of IL-adsorbed TiO_2 surfaces with the aim of providing fundamental information about how the IL environment affects the preferred shape and exposed facet of TiO_2 crystals. In order to make progress toward this goal, we first examine the adsorption energies and geometries of a typical IL ([Emim]Br) on TiO_2 facets to determine its most preferred adsorption facets. Our calculated result shows that [Emim]Br prefers to adsorb on (110) for rutile and (100) for anatase. After [Emim]Br adsorption, the surface energy gap shows an obvious increase between the anatase (101) and (001) surfaces as well as between the rutile (110) and (001) surfaces. Based on our calculated surface energies and Wulff's rule, the equilibrium shapes of TiO_2 crystals were obtained. We found that this variation of surface energy gap results in increasing the (100) facet exposure of anatase and also increases in the length-to-diameter ratio of rutile nanocrystals. For comparison, a number of calculations of H^+ and H_2O adsorption were performed to investigate the effects of acidic and neutral aqueous environment on the TiO_2 morphologies. We note that this work not only allows us to obtain a profound understanding of how to achieve shape-directed nanocrystal synthesis by using ILs as the controlling agents but also shows that starting by surface chemistry is a helpful approach to predict the morphology transformation of the nanocrystals. The results will be a significant step toward the ultimate goal of controlling synthesis of inorganic nanomaterials to generate functional materials, ultimately of relevance for real applications.

2. COMPUTATIONAL METHOD AND DETAILS

All calculations were performed using the DFT package VASP,[18,19] where we employ the generalized gradient approximation by the functional of Perdew and Wang (GGA-PW91).[20] The electron−ion interaction is described by the projector-augmented wave (PAW) scheme,[21,22] and for the plane wave set a cutoff energy of 400 eV was used in all the computations. The rutile and anatase phase TiO_2 was chosen as the research object, because the rutile phase is the thermodynamically stable phase of TiO_2 at the macroscale[23] and th anatase phase is the thermodynamically stable phase at the nanoscale.[24] Our optimized lattice constants of bulk rutile ($a = b = 4.602$ Å and $c = 2.965$ Å) and anatase ($a = b = 3.783$ Å and $c = 9.491$ Å) are in good agreement with the previous results.[25] The surfaces were modeled by a periodical array of six atomic layers separated by 15 Å of vacuum region. Here, we consider the low-index facets of TiO_2, namely, the (101), (100), and (001) anatase facets and (110), (101), and (001) rutile facets. For surfaces adsorption, $p(2 \times 2)$ for rutile (110), (101), and (001) facets has been considered, corresponding to a 1/4 monolayer coverage for single adsorbate on these surfaces. And $p(2 \times 2)$ for anatase (100), (101), and (001) facets has been considered, corresponding a a coverage of 1/4 monolayer for single adsorbate adsorption for these surfaces. In calculation, the adsorbate and the first three atom layers are allowed to relax, whereas the bottom layers of the slab are fixed. Spin-polarized calculations were performed when needed. The Brillouin-zone integrations have been performed using a $2 \times 2 \times 1$ Monkhorst−Pack grid which was tested to be a reasonable *k*-points grid.[26] The structural optimization is performed with a termination criterion of 0.05 eV/Å for atomic forces. The semiempirical dispersion terms, parametrized by Grimme,[27] and applied for modeling the interactions between adsorbed molecules and metal oxide substrates, were added to the quantum mechanical energies and gradients (called the DFT+*D* method).

In this study, the clean, H_2O-, H^+- and IL-adsorbed facets were used to simulate the ideal, water, acidic, and IL environments, respectively. The adsorption energy (E_{ads}) is calculated according to the formula: $E_{ads} = E_{adsorbate/slab} - E_{adsorbate} - E_{slab}$, where $E_{adsorbate/slab}$, $E_{adsorbate}$, and E_{slab} are the energies of the whole adsorption system, isolated adsorbate molecule, and surface slab, respectively. The surface energy (γ) is calculated as follows: $\gamma = (E_{slab} - mE_{unit})/2A$, where E_{slab} is the energy of the surface slab, E_{unit} is the average energy per TiO_2 unit in the bulk, m represents the numbers of TiO_2 units, and A is the surface area. Because only one surface is allowed to relax with the bottom layers of the slab fixed, the coefficient before A is unity. Thus, the surface energy is given as $\gamma = (E_{slab} - mE_{unit})/A$. The surface energy of the surfaces with adsorbed species is defined as $\gamma = (E_{adsorbate/slab} - E_{adsorbate} - mE_{unit})/A$, where $E_{adsorbate/slab}$ is the energy of the TiO_2 surface with adsorbed species; $E_{adsorbate}$ is the energy of an isolated adsorbate molecule. In this work, the equilibrium shape of a crystal is obtained by minimizing the surface energy for a fixed volume according to the Wulff's rule.[28] The Wulff's rule can be expressed as $\gamma(hkl)/d(hkl) =$ constant, where $\gamma(hkl)$ is the surface energy of the (hkl) facet and $d(hkl)$ is the distance from the center of the crystal to the (hkl) facet.

3. RESULTS AND DISCUSSION

3.1. Isolated [Emim]$^+$ and [Emim]Br. Figure 1 shows the optimized structures of the isolated [Emim]$^+$ and [Emim]Br obtained by a $16 \times 16 \times 16$ Å^3 box. The structure of [Emim]$^+$ shows that the C_2−H_{NHC} bond length is 1.09 Å, which agrees well with 1.08 Å obtained by Andrade et al.[29] and 1.07 Å by Ghatee and Moosavi[30] (C_2, C atom at position 2 of the imidazolium ring; H_{NHC}, the H atom in the C2 position). The

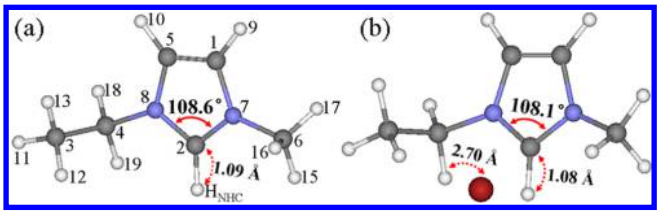

Figure 1. Optimized structures of (a) isolated [Emim]$^+$ and (b) [Emim]Br. Atoms are presented as deep gray (C), sky-blue (N), white (H), and deep red (Br).

dx.doi.org/10.1021/jp503891s | J. Phys. Chem. C 2014, 118, 23320−23327

bond angle of $\angle NC_2N$ is 108.6°, which is consistent with the previous calculated results.[31] ($\angle NC_2N$, the angle between two N−C_2 bonds). For the [Emim]Br ionic pair, the structure of $[Emim]^+$ is slightly changed from its isolated state because of the mutual interactions with Br^-. The C_2−H_{NHC} bond length changes to 1.08 Å, and $\angle NC_2N$ is 108.1°. The nearest $Br^-\cdots H$ distance is 2.70 Å, which is consistent with 2.72 Å obtained by Allen et al.[32] and 2.60 Å by Tsuzuki et al.[33] The charge distribution by Bader analysis shows that a charge of 0.2684 *e* is transferred from Br^- to $[Emim]^+$, as compared to 0.2750 *e* reported by Valencia et al.[34] The charge of C_2 decrease slightly from +2.2249 to +2.1324 *e*, and the charge of H_{NHC} decrease from +0.4634 to +0.3694 *e*, which may increase H_{NHC} bonding ability.

3.2. Anatase Surfaces. Usually, TiO_2 crystals grow at an acidic environment,[35] and the pH is lower than its isoelectric point (IEP = 6);[36] thus the cation adsorptions (e.g., H^+ and $[Emim]^+$) should be considered first. Figure 2 shows that

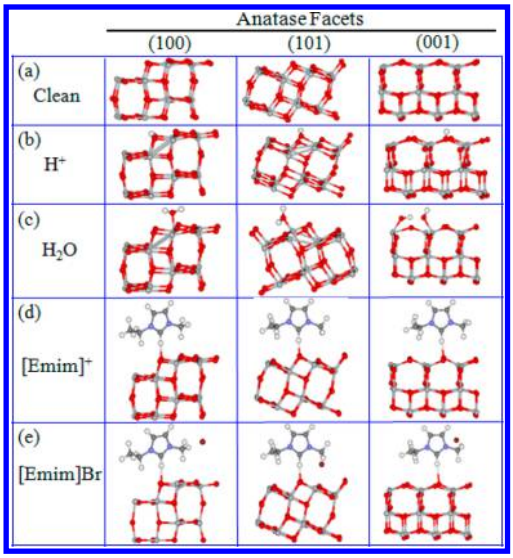

Figure 2. Optimized structures of (a) a clean surface and (b) H^+, (c) H_2O, (d) $[Emim]^+$, and (e) [Emim]Br adsorbed on the (100), (101), and (001) anatase surfaces. Atoms are presented as gray (Ti), red (O), deep gray (C), sky-blue (N), white (H), and deep red (Br). (Note: Corresponding geometrical parameters are listed in Table S1, Supporting Information.)

$[Emim]^+$ prefers to vertically adsorb on anatase surfaces, through forming a H_{NHC}−O bond, which is consistent with adsorption models on metal surfaces.[37] The bond length of H_{NHC}−O is in the common range of hydrogen bond length (1.5−2.5 Å),[38] which indicates that the interaction between $[Emim]^+$ and the surface is mainly through hydrogen bond and electrostatic interactions. Besides, the distance between H_{NHC} and the surface O was smaller than the sum of the van der Waals radius of H and O atoms (2.6 Å), also indicating the formation of a hydrogen bond. This interaction is similar to that of $[C_4C_1Im]^+$ on Al_2O_3 (100) simulated by Martins et al.[39] On anatase (101), $[Emim]^+$ adsorbs at the top site of the O atom with H_{NHC}−O bond length of 1.63 Å. The C_2−H_{NHC} bond length changes to 1.14 Å, and $\angle NC_2N$ is 107.7°. On anatase (100), the O atom is still attracted toward H_{NHC} atom, with the O−H_{NHC} bond length of 1.85 Å. The C_2−H_{NHC} bond length changes to 1.11 Å, and $\angle NC_2N$ is 108.2°. On anatase (001), $[Emim]^+$ binds to O through forming an O−H_{NHC} bond (1.80 Å). The C_2−H_{NHC} bond length changes to 1.13 Å, and $\angle NC_2N$ is 107.2°. Table 1 lists the adsorption energies of $[Emim]^+$ on anatase (101), (100), and (001) as −1.46, −1.41, and −1.24 eV, respectively, indicating that $[Emim]^+$ has a relatively weaker adsorption on the (001) surface.

Consequently, Br^- anions may move to the surface and achieve an electrostatic equilibrium with $[Emim]^+$ cations. As a result, an electrostatic layer is formed at the surface, which is similar to the Derjaugin−Landau−Verwey−Overbeek (DLVO) model.[40] To confirm the stable configuration of [Emim]Br/TiO_2 (Figure 2), we optimize the location of Br^- based on the stable position of $[Emim]^+$ that has been obtained previously. Table 1 lists adsorption energies of [Emim]Br on anatase (101), (100), and (001) as −1.02, −1.11, and −0.99 eV, indicating that [Emim]Br prefers to adsorb on (100). For [Emim]Br adsorbed on anatase (101), $[Emim]^+$ is at the top site of the O atom, with the H_{NHC}−O distance of 1.87 Å. The C_2−H_{NHC} bond length changes to 1.10 Å, and $\angle NC_2N$ is 108.1°. Br^- adsorbs at the near top site of Ti atom, with the $Br^-\cdots$Ti distance of 3.25 Å. For [Emim]Br adsorbed on anatase (100), the O atom is still attracted toward H_{NHC}, and O−H_{NHC} bond length is 2.39 Å. The C_2−H_{NHC} bond length changes to 1.09 Å, and $\angle NC_2N$ is 108.5°. Br^- is at the top site of the Ti atom, with the $Br^-\cdots$Ti distance of 3.71 Å. For $[Emim]^+$ adsorbed on anatase (001), H_{NHC} links to the O atom with an O−H_{NHC} bond length of 2.33 Å. The C_2−H_{NHC} bond length changes to 1.09 Å, and $\angle NC_2N$ is 108.3°. The Br^- is at the top site of Ti, with the $Br^-\cdots$Ti distance of 3.64 Å. After adsorption, the [Emim]Br occurs as a tiny distortion and this small geometric change will induce the energy changing for these ILs themselves, which will have important implications for the surface energy of the whole adsorption system. The surface energies of [Emim]Br-adsorbed anatase surfaces are 1.36, 1.39, and 1.75 J/m^2 for (101), (100), and (001), respectively.

Experimentally, the hydrothermal method is commonly used in synthesis TiO_2 under acidic condition. The hydrated surface region confined and/or bonded H_2O molecules and/or H^+ species and is unavoidable. Thus, to investigate the adsorption of H_2O and H^+ on TiO_2 facets is necessary. The optimized structures are shown in Figure 2, and corresponding energetic data are listed in Table 1. The adsorption energy of H_2O is −0.70 eV for anatase (101), with Ti−H_2O bond length of 2.31 Å, and −0.61 eV for (100), with Ti−H_2O bond length of 2.33

Table 1. Results of Adsorption of $[Emim]^+$, [Emim]Br, H_2O, and H^+ on Anatase (101), (100), and (001) Facets, Adsorption Energy [$E_{ads}^{[Emim]^+}$, $E_{ads}^{[Emim]Br}$, $E_{ads}^{H_2O}$, and $E_{ads}^{H^+}$ (eV)] for $[Emim]^+$, [Emim]Br, H_2O, and H^+ Adsorption and Surface Energy [γ^{pure}, γ^{H_2O}, γ^{H^+}, $\gamma^{[Emim]^+}$, and $\gamma^{[Emim]Br}$ (J/m^2)] for Pure and H_2O-, H^+-, $[Emim]^+$-, and [Emim]Br-Adsorbed Facets

anatase facet	γ^{pure}	γ^{H_2O}	γ^{H^+}	$\gamma^{[Emim]^+}$	$\gamma^{[Emim]Br}$	$E_{ads}^{H_2O}$	$E_{ads}^{H^+}$	$E_{ads}^{[Emim]^+}$	$E_{ads}^{[Emim]Br}$
(101)	1.57	1.43	1.12	1.27	1.36	−0.70	−2.21	−1.46	−1.02
(100)	1.64	1.50	1.16	1.32	1.39	−0.61	−2.12	−1.41	−1.11
(001)	1.94	1.57	1.40	1.70	1.75	−1.98	−2.85	−1.24	−0.99

dx.doi.org/10.1021/jp503891s | J. Phys. Chem. C 2014, 118, 23320−23327

Å (Ti−H_2O, the bond between the O of H_2O and Ti). Different from the (101) and (100) surfaces, the H_2O adsorption on (001) is not as molecular (H_2O) but as an ion group (OH^- and H^+), which is consistent with that in the reported literature.[41] The adsorption energy is −1.98 eV, with a Ti−OH^- bond length of 1.86 Å and O−H^+ of 1.04 Å. The surface energy of H_2O-adsorbed facets is 1.43, 1.50, and 1.57 J/m^2 for (101), (100), and (001). For the clean surface, the order of surface energy is 1.57 J/m^2 (101) < 1.64 J/m^2 (100) < 1.94 J/m^2 (001). The surface energy of H^+-adsorbed anatase facets is 1.12, 1.16, and 1.40 J/m^2 for (101), (100), and (001), which is consistent with the results from Barnard et al.[42] It is obvious that the surface energy of these surfaces is also reduced after adsorption of H_2O or H^+.

For further investigating the effect of surface energetics on crystal shape, according to Wulff's rule and our calculated surface energies (Table 1), we obtain the equilibrium shape of anatase nanocrystals under each type of surface chemistry environment (Figure 3). Under an ideal environment, the

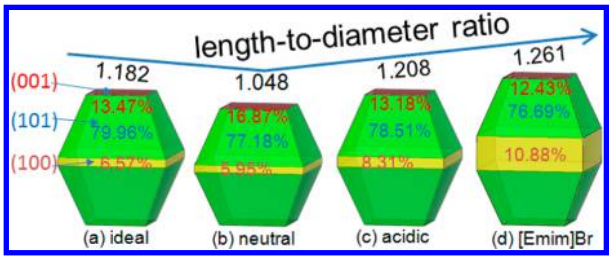

Figure 3. Predicted equilibrium shapes and relative contribution of each facet of anatase nanocrystals determined from Wulff's rule using the calculated surface energies under the conditions of (a) ideal, (b) neutral water, (c) acidic solution, and (d) [Emim]Br. Red is for (001), blue is for (101), and brown for (100) facet.

bipyramid shape of anatase crystal has a length-to-diameter ratio of 1.182. 79.96% of the crystal surface is occupied by (101) facet and (001) facet contributes 13.47% at the bottom and top of the crystals. Only 6.57% of the crystal shape is occupied by (100) facet. Under neutral aqueous environment, 77.18% and 5.95% are occupied by (101) and (100) facets, respectively. (001) facet has a contribution of 16.87% at the bottom and top of the crystals. The length-to-diameter ratio of the anatase bipyramid shape is 1.048. Under the acidic environment, the length-to-diameter ratio of the bipyramid is up to 1.208. 78.51% of the total surface area is occupied by the (101) facet; the ratio of (100) facets is increased to 8.31%, and the ratio of (001) facets is decreased to 13.18%. Comparing the neutral and acidic environments discussed earlier, it is also possible to explain the experimental observation in synthesis of anatase nanocrystals: low pH values tended to eliminate (001) facets by forming sharp corners, and the length-to-diameter ratio increased.[43] We suggested that this could be caused by the H_2O (dissociated as OH^- and H^+) adsorption on (001) facets which is a high energy surface. The free energy release of the H_2O adsorption is larger than (101) and (100), which can reduce the surface energy of (001) markedly. At this condition, the surface energy gap between (100) and (001) is smaller than that of H^+ adsorption. As a result, the sharper nanocrystals will be synthesized at relatively low pH conditions. However, under an environment containing [Emim]Br, the bipyramid shows an obvious elongation along the [001] direction and the length-to-diameter ratio is up to 1.261. The contribution of the (101) facet is decreased to 76.69%, whereas the (100) surface is increased to 10.88%, and the contribution of the (001) facet to the total surface area was decreased to 12.43%. It is clear to see that the surface energetics has a fairly obvious effect on the shape and exposed facet of anatase nanocrystals.

Based on the preceding calculations, we can see that the gap of surface energy for the [Emim]Br-adsorbed anatase surfaces shows an obvious increase compared with the case of H^+ adsorption, especially between the anatase (100) and (001) surfaces. In the growth environment containing [Emim]Br, the Wulff crystal shape shows that this gap variation of the surface energy results in increasing the (100) facet exposure of anatase and also increasing the length-to-diameter ratio, in comparison with the H^+ and H_2O-adsorbed conditions.

3.3. Rutile Surfaces. Just like on the anatase surfaces, $[Emim]^+$ also prefers to vertically adsorb on rutile surfaces, through forming hydrogen bond and electrostatic interaction (Figure 4). On rutile (110), $[Emim]^+$ adsorbs at the top site of

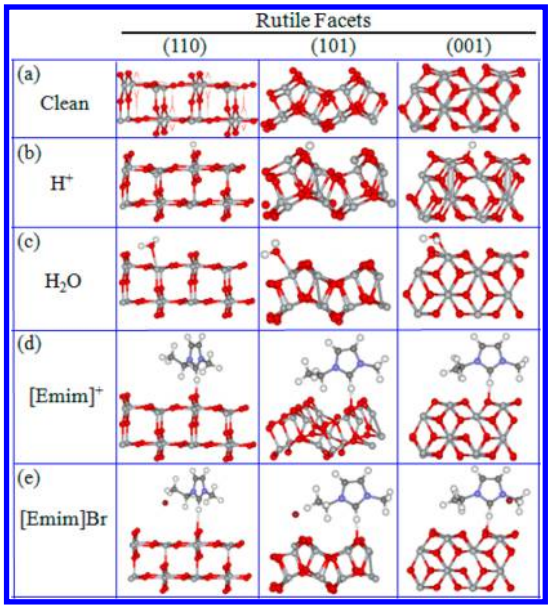

Figure 4. Optimized structures of (a) a clean surface and (b) H^+, (c) H_2O, (d) $[Emim]^+$, and (e) [Emim]Br adsorbed on the (110), (101), and (001) rutile surfaces. Atoms are presented as gray (Ti), red (O), deep gray (C), sky-blue (N), white (H), and deep red (Br). (Note: Corresponding geometrical parameters are listed in Table S2, Supporting Information.)

the bridge O atom with an O−H_{NHC} bond length of 1.87 Å. The C_2−H_{NHC} bond length changes to 1.11 Å, and ∠NC_2N is 106.9°. On rutile (101), H_{NHC} still binds to bridge O and the O−H_{NHC} bond length is 1.69 Å. The C_2−H_{NHC} bond length elongates to 1.13 Å, and ∠NC_2N increases to 107.3°. On rutile (001), $[Emim]^+$ through its H_{NHC} links to O, with an O−H_{NHC} bond length of 1.81 Å. In the adsorbed $[Emim]^+$, the C_2−H_{NHC} bond length changes to 1.11 Å and ∠NC_2N is 107.1°. The adsorption energy of $[Emim]^+$ is −1.56, −1.46, and −1.06 eV on rutile (110), (101), and (001) (Table 2), which indicates that $[Emim]^+$ prefers to adsorb on rutile (110). This adsorption selectivity may be caused by the rutile surface structure difference. As shown in Figure 4, there is a cave between the two neighboring rows of bridge O atoms on rutile (110), which contribute $[Emim]^+$ tilt and, close to (110), contribute strong

dx.doi.org/10.1021/jp503891s | J. Phys. Chem. C 2014, 118, 23320−23327

Table 2. Results of Adsorption of $[Emim]^+$, [Emim]Br, H_2O, and H^+ on Rutile (110), (101), and (001) Facets, Adsorption Energy [$E_{ads}^{[Emim]^+}$, $E_{ads}^{[Emim]Br}$, $E_{ads}^{H_2O}$, and $E_{ads}^{H^+}$ (eV)] for $[Emim]^+$, [Emim]Br, H_2O, and H^+ Adsorption and Surface Energy [γ^{pure}, γ^{H_2O}, γ^{H^+}, $\gamma^{[Emim]^+}$, and $\gamma^{[Emim]Br}$ (J/m^2)] for Pure and H_2O-, H^+-, $[Emim]^+$-, and [Emim]Br-Adsorbed Facets

rutile facet	γ^{pure}	γ^{H_2O}	γ^{H^+}	$\gamma^{[Emim]^+}$	$\gamma^{[Emim]Br}$	$E_{ads}^{H_2O}$	$E_{ads}^{H^+}$	$E_{ads}^{[Emim]^+}$	$E_{ads}^{[Emim]Br}$
(110)	1.06	0.89	0.59	0.73	0.77	−0.77	−2.22	−1.56	−1.33
(101)	1.73	1.59	1.30	1.49	1.55	−0.85	−2.66	−1.46	−1.10
(001)	2.85	2.67	2.42	2.66	2.65	−0.98	−2.31	−1.06	−1.05

hybridization effects for electron clouds, and occurs as a stronger interaction with the (110) surface.

Figure 4 shows the optimized structure of [Emim]Br on rutile surfaces, and corresponding energetic data are listed in Table 2. On rutile (110), $[Emim]^+$ adsorbs on the top site of the bridge O atom with the O−H_{NHC} bond length of 2.15 Å, and the adsorption energy is −1.56 eV. The C_2−H_{NHC} bond length of the adsorbed $[Emim]^+$ changes to 1.10 Å, and ∠NC_2N is 107.9°. Br^- is at the top site of Ti, with the Br^-···Ti distance of 3.01 Å. On rutile (101), the adsorption energy of [Emim]Br is −1.46 eV. For the adsorbed $[Emim]^+$, H_{NHC} atom still binds to surface O and forms the O−H_{NHC} bond length with 2.06 Å. The C_2−H_{NHC} bond length is 1.11 Å, and ∠NC_2N is 107.9°. The Br^-···Ti distance is 2.77 Å. On rutile (001), the adsorption energy of [Emim]Br is −1.06 eV with the H_{NHC}−O length of 2.17 Å. The C_2−H_{NHC} bond length of adsorbed $[Emim]^+$ changes to 1.09 Å, and ∠NC_2N is 108.1°. Br^- locates at the near top site of Ti, and the Br^-···Ti distance is 2.96 Å. For [Emim]Br-adsorbed surfaces, the surface energies are 0.77, 1.55, and 2.65 J/m^2 for the rutile (110), (101), and (001) surfaces.

The H^+- and H_2O-adsorbed rutile facets are as shown in Figure 4. For H_2O-adsorbed rutile (110), the adsorption energy is −0.77 eV with a Ti−H_2O bond length of 2.25 Å. The adsorption energies are −0.85 and −0.98 eV for H_2O-adsorbed rutile (101) and (001), and corresponding Ti−H_2O bond lengths are 2.21 and 2.16 Å. The surface energies of H_2O-adsorbed facets are 0.89, 1.59, and 2.67 J/m^2 for (110), (101), and (001). The surface energies of H^+-adsorbed facets are 0.59, 1.30, and 2.42 J/m^2 for (110), (101), and (001). We can see that H^+ can effectively protect the facets and decrease surface energy, but the gap of the surface energy between (110) and (001) is not enlarged.

Figure 5 shows the Wulff crystal shape of rutile obtained according to our calculated surface energies. Under an ideal environment, the rod-like rutile nanocrystal has a length-to-diameter ratio of 1.931. 67.90% of the crystal shape is occupied by the (110) facet, and the (101) facet has a contribution of 32.09%. (001) has a very small contribution to the total surface due to the high surface energy. Under a neutral aqueous environment, the rutile rod has a length-to-diameter ratio of 2.108. 70.79% of the crystal shape is occupied by the (110) facet, and the (101) facet has a contribution of 29.20%. Under the acidic environment, the length-to-diameter ratio of the rutile rod is up to 2.221. 72.37% of the total surface area is occupied by the (110) facet. The (101) facet has a contribution of 27.62%. Under the environment containing [Emim]Br, the rutile rod becomes elongated and the length-to-diameter ratio is increased to 2.368. The contribution of the (110) surface to the total surface area is up to 74.20%, the (101) facet is down to 25.79%, and (001) facets have a small ratio. Obviously, the [Emim]Br effectively promotes rutile crystals of one-dimensional growth along the [001] direction and form longer rutile nanorods.

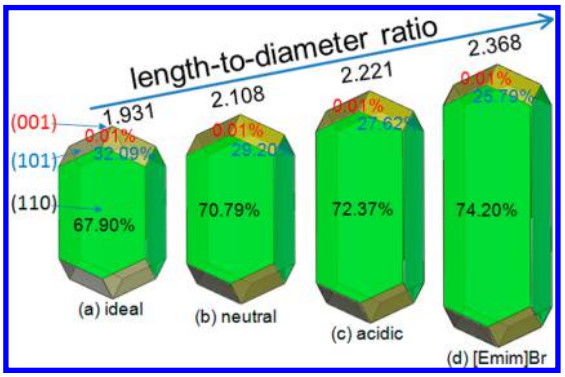

Figure 5. Predicted equilibrium shapes and relative contribution of each facet of rutile nanocrystals determined from Wulff's rule using the calculated surface energies under the conditions of (a) ideal, (b) neutral water, (c) acidic solution, and (d) [Emim]Br. Red is for (001) facet, blue is for (101) facet, and black is for (110) facet.

These simulations show that the surface energies of rutile facets are greatly reduced after adsorption of H^+, H_2O, and [Emim]Br. Compared to the adsorption of H^+ (or H_2O) on the rutile surfaces, the adsorption of [Emim]Br effectively enlarged the surface energy gap between (001) and (110), based on Wulff's rule, which contributes to longer rod-like rutile nanocrystals with a large exposure of (110) facets.

4. COMPARISON WITH EXPERIMENT

In order to obtain further experimental support for the theoretically predicted morphology control of TiO_2 nanocrystals in the IL growth environment, comparison experiments were carried out. At the growth environments containing ILs, TiO_2 nanocrystals were prepared by hydrothermal synthesis (Experimental Details are presented in the Supporting Information). As shown in Figure 6, all X-ray diffraction (XRD) patterns of the as-prepared samples can be indexed to the rutile TiO_2 (JCPDS No. 21-1276). The strong diffraction peaks reveal the good crystallinity of the two samples. A close examination shows that at the growth environment containing [Emim]Br, the ratio of the relative intensity of (110)/(002) diffractions shows a slightly increasing trend when compared to that of no addition of ILs (7.5 vs 5.3). This trend is expected when considering the increasing fractions of (110) facets.

To further confirm the morphologies of rutile nanocrystals, detailed transmission electron microscopy (TEM) analysis has been performed on the products synthesized, as shown in Figure 7. With no [Emim]Br added, the length-to-diameter ratio of rutile nanorods is ∼2.5. The diameter of the nanorods is 20−25 nm, and the length is 50−55 nm. The corresponding high-resolution (HRTEM) image exhibits lattice spacing of ∼0.33 nm, corresponding to the (110) plane, which indicates [001] is the growth direction of rutile nanorods. When added

dx.doi.org/10.1021/jp503891s | J. Phys. Chem. C 2014, 118, 23320−23327

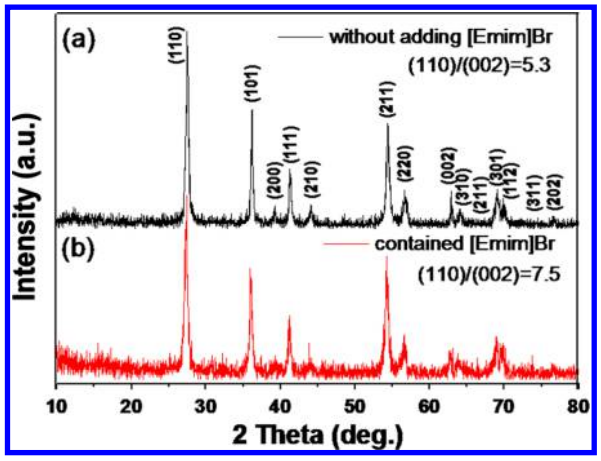

Figure 6. XRD patterns of rutile nanocrystals prepared under the growth environments (a) without adding [Emim]Br and (b) containing [Emim]Br. The increase in the (110)/(002) ratio indicates a clear trend toward larger (110) faceting for rutile nanocrystals produced with the assistance of [Emim]Br.

[Emim]Br to the reaction solution, the rutile formed a sharper nanorod and exhibited a higher length-to-diameter ratio, ~5.0. The rod diameter is decreased to 15−25 nm while its length is increased to 100−125 nm. The lattice spacing of ~0.33 nm is well indexed to the (110) plane, which indicates that the rutile nanorods grow along the [001] direction and its dominating side surfaces are (110) planes. These preceding structural characterization results demonstrate that the growth environment containing [Emim]Br not only induces a higher length-to-diameter ratio of rutile nanocrystals but also increases the contribution of (110) exposed facets. From the DFT+*D* calculated results, we know that the surface energy of rutile (110) reduces much more than that of (101) and (001) after adsorption of [Emim]Br. According to Wulff's rule, the more decrease in the surface energy of (110), the shorter the distance between (110) and the center, whereas the distance of (001) to the center is longer. However, at the cases of H^+ or H_2O adsorption, the gap of the surface energy between (110) and (001) is smaller than that of [Emim]Br adsorption. Thus, the equilibrium crystal shape grown at IL assistance should own a higher length-to-diameter ratio and larger exposed facet of (110).

Similar experimental results have also been observed in the synthesis of anatase nanocrystals. One typical example is that Qi et al.,[10] using [Emim]Br as a capping agent, successfully prepared cube-shape anatase nanocrystals with the dominating (100) exposed facet. Similar results were also obtained by Liu et al. in the synthesis bipyramid-shaped anatase nanocrystals by using a microwave method.[11] Based on our calculated results, we can give a reasonable explanation for this phenomenon about anatase shape evolution. The main reason is that [Emim]Br selective adsorption on anatase (100) effectively decreases the surface energy and protects this facet. In comparison with H^+ (or H_2O)-adsorbed conditions, the gap of the surface energy between the [Emim]Br-adsorbed anatase (100) and (001) facets shows an obvious increase. This gap variation of surface energy contributes to the cubic-shape formation with a large ratio of (100) facet exposure according to Wulff's rule.

5. CONCLUSION

In order to provide fundamental information on how an ionic liquid environment affects TiO_2 morphologies, DFT+*D* calculations were performed to study the surface chemistry of IL-adsorbed TiO_2 facets. The equilibrium shapes of TiO_2 nanocrystals were derived from our calculated surface energies based on Wulff's rule. The ionic liquid [Emim]Br can effectively decrease the surface energy of TiO_2 facets, especially for the anatase (100) and rutile (110) facets, resulting in an increase in the ratio of the (100) exposed facets of anatase and an increase in the length-to-diameter ratio of rutile nanocrystals. These DFT+*D* calculated results also get a further support from our experiment. We hope that our work is beneficial for getting a

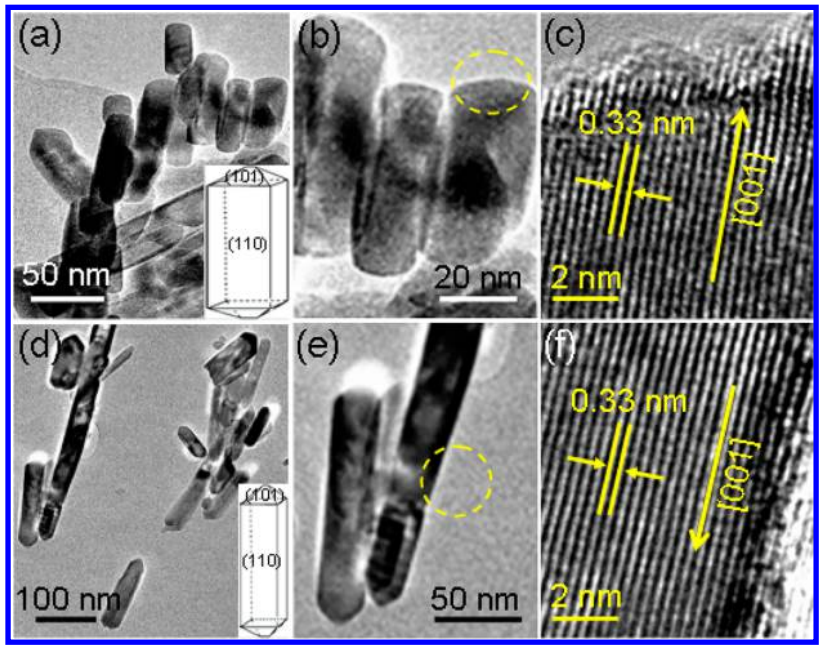

Figure 7. TEM and corresponding HRTEM images of rutile TiO_2 nanocrystals prepared under the growth environment: (a−c) without adding [Emim]Br; (d−f) contained [Emim]Br. Insets: Schematic drawing of the morphology of rutile nanocrystals.

dx.doi.org/10.1021/jp503891s | J. Phys. Chem. C 2014, 118, 23320−23327

profound understanding of how to achieve shape-controlled synthesis of nanomaterials by IL assistance.

■ ASSOCIATED CONTENT

Supporting Information

Text describing details of the synthesis procedure and tables listing important geometrical parameters. This material is available free of charge via the Internet at http://pubs.acs.org.

■ AUTHOR INFORMATION

Corresponding Authors

*(W.Z.) E-mail: zhwj@nankai.edu.cn.

*(G.W.) E-mail: wangguichang@nankai.edu.cn.

Notes

The authors declare no competing financial interest.

■ ACKNOWLEDGMENTS

This work was supported by the National Natural of Science Foundation of China (Grant Nos. 21073095 and 21371101), the 111 Project (Grant No. B12015), and the MOE Innovation Team (Grant No. IRT13022) of China. We are highly grateful to Dr. Weiliu Fan for many valuable discussions.

■ REFERENCES

(1) Hoffmann, M. R.; Martin, S. T.; Choi, W.; Bahnemann, D. W. Environmental Applications of Semiconductor Photocatalysis. *Chem. Rev.* **1995**, *95*, 69−96.

(2) Qi, K. Z.; Yang, J. Q.; Fu, J. Q.; Wang, G. C.; Zhu, L. J.; Liu, G.; Zheng, W. J. Morphology-controllable ZnO rings: Ionic liquid assisted hydrothermal synthesis, growth mechanism and photoluminescence properties. *CrystEngComm* **2013**, *15*, 6729−6735.

(3) Joo, J.; Kwon, S. G.; Yu, T.; Cho, M.; Lee, J.; Yoon, J.; Hyeon, T. Large-Scale Synthesis of TiO_2 Nanorods via Nonhydrolytic Sol−Gel Ester Elimination Reaction and Their Application to Photocatalytic Inactivation of *E. coli*. *J. Phys. Chem. B* **2005**, *109*, 15297−15302.

(4) Murakami, N.; Kurihara, Y.; Tsubota, T.; Ohno, T. Shape-Controlled Anatase Titanium(IV) Oxide Particles Prepared by Hydrothermal Treatment of Peroxo Titanic Acid in the Presence of Polyvinyl Alcohol. *J. Phys. Chem. C* **2009**, *113*, 3062−3039.

(5) Cozzoli, P. D.; Kornowski, A.; Weller, H. Low-temperature synthesis of soluble and processable organic-capped anatase TiO_2 nanorods. *J. Am. Chem. Soc.* **2003**, *125*, 14539−14548.

(6) Ma, Z.; Yu, J. H.; Dai, S. Preparation of Inorganic Materials Using Ionic Liquids. *Adv. Mater.* **2010**, *22*, 261−285.

(7) Zhou, Y.; Schattka, J. H.; Antonietti, M. Room-Temperature Ionic Liquids as Template to Monolithic Mesoporous Silica with Wormlike Pores via a Sol−Gel Nanocasting Technique. *Nano Lett.* **2004**, *4*, 477−481.

(8) Zheng, W. J.; Liu, X. D.; Yan, Z. Y.; Zhu, L. J. Ionic Liquid-Assisted Synthesis of Large-Scale TiO_2 Nanoparticles with Controllable Phase by Hydrolysis of $TiCl_4$. *ACS Nano* **2009**, *3*, 115−122.

(9) Zhou, Y.; Antonietti, M. Synthesis of Very Small TiO_2 Nanocrystals in a Room-Temperature Ionic Liquid and Their Self-Assembly toward Mesoporous Spherical Aggregates. *J. Am. Chem. Soc.* **2003**, *125*, 14960−14961.

(10) Zhao, X. W.; Jin, W. Z.; Cai, J. G.; Ye, J. F.; Li, Z. H.; Ma, Y. R.; Xie, J. L.; Qi, L. M. Shape- and Size-Controlled Synthesis of Uniform Anatase TiO_2 Nanocuboids Enclosed by Active {100} and {001} Facets. *Adv. Funct. Mater.* **2011**, *21*, 3554−3563.

(11) Ding, K. L.; Miao, Z. J.; Liu, Z. M.; Zhang, Z. F.; Han, B. X.; An, G. M.; Miao, S. D.; Xie, Y. Facile Synthesis of High Quality TiO_2 Nanocrystals in Ionic Liquid via a Microwave-Assisted Process. *J. Am. Chem. Soc.* **2007**, *129*, 6362−6363.

(12) Wender, H.; Feil, A. F.; Diaz, L. B.; Ribeiro, C. S.; Machado, G. J.; Migowski, P.; Weibel, D. E.; Dupont, J.; Teixeira, S. R. Self-Organized TiO_2 Nanotube Arrays: Synthesis by Anodization in an Ionic Liquid and Assessment of Photocatalytic Properties. *ACS Appl. Mater. Interfaces* **2011**, *3*, 1359−1365.

(13) Piskorz, W.; Grybos, J.; Zasada, F.; Zapała, P.; Cristol, S.; Paul, J.-F.; Sojka, Z. Periodic DFT Study of the Tetragonal ZrO_2 Nanocrystals: Equilibrium Morphology Modeling and Atomistic Surface Hydration Thermodynamics. *J. Phys. Chem. C* **2012**, *116*, 19307−19320.

(14) Yang, H. G.; Sun, C. H.; Qiao, S. Z.; Zou, J.; Liu, G.; Smith, S. C.; Cheng, H. M.; Lu, G. Q. Anatase TiO_2 single crystals with a large percentage of reactive facets. *Nature* **2008**, *453*, 638−641.

(15) Barnard, A. S.; Zapol, P.; Curtiss, L. A. Modeling the Morphology and Phase Stability of TiO_2 Nanocrystals in Water. *J. Chem. Theory Comput.* **2005**, *1*, 107−116.

(16) Mercurio, G.; McNellis, E. R.; Martin, I.; Hagen, S.; Leyssner, F.; Soubatch, S.; Meyer, J.; Wolf, M.; Tegeder, P.; Tautz, F. S.; Reuter, K. Structure and Energetics of Azobenzene on Ag(111): Benchmarking Semiempirical Dispersion Correction Approaches. *Phys. Rev. Lett.* **2010**, *104*, 036102-1−036102-4.

(17) Godlewski, S.; Tekiel, A.; Piskorz, W.; Zasada, F.; Prauzner-Bechcicki, J. S.; Sojka, Z.; Szymonski, M. Supramolecular Ordering of PTCDA Molecules: The Key Role of Dispersion Forces in an Unusual Transition from Physisorbed into Chemisorbed State. *ACS Nano* **2012**, *6*, 8536−8545.

(18) Kresse, G.; Hafner, J. *Ab initio* molecular-dynamics simulation of the liquid-metal-amorphous-semiconductor transition in germanium. *Phys. Rev. B* **1994**, *49*, 14251−14269.

(19) Kresse, G.; Furthmüller, J. Efficiency of *ab-initio* total energy calculations for metals and semiconductors using a plane-wave basis set. *Comput. Mater. Sci.* **1996**, *6*, 15−50.

(20) Perdew, J. P.; Chevary, J. A.; Vosko, S. H.; Jackson, K. A.; Pederson, M. R.; Singh, D. J.; Fiolhais, C. Atoms, molecules, solids, and surfaces: Applications of the generalized gradient approximation for exchange and correlation. *Phys. Rev. B* **1992**, *46*, 6671−6687.

(21) Blöchl, P. E. Projector augmented-wave method. *Phys. Rev. B* **1994**, *50*, 17953−17979.

(22) Kresse, G.; Joubert, D. From ultrasoft pseudopotentials to the projector augmented-wave method. *Phys. Rev. B* **1999**, *59*, 1758−1775.

(23) Muscat, J.; Swamy, V.; Harrison, N. M. First-principles calculations of the phase stability of TiO_2. *Phys. Rev. B* **2002**, *65*, 224112−224126.

(24) Levchenko, A. A.; Li, G.; Boerio-Goates, J.; Woodfield, B. F.; Navrotsky, A. TiO_2 Stability Landscape: Polymorphism, Surface Energy, and Bound Water Energetics. *Chem. Mater.* **2006**, *18*, 6324−6332.

(25) Diebold, U. The surface science of tianium dioxide. *Surf. Sci. Rep* **2003**, *48*, 53−229.

(26) Monkhorst, H. J.; Pack, J. D. Special points for Brillouin-zone integrations. *Phys. Rev. B* **1976**, *13*, 5188−5192.

(27) Grimme, S. Accurate Description of van der Waals Complexes by Density Functional Theory Including Empirical Corrections. *J. Comput. Chem.* **2004**, *25*, 1463−1473.

(28) Wulff, G. Zur Frage der Geschwindigkeit des Wachstums und der Auflösung der Krystallflagen. *Z. Kristallogr. Mineral.* **1901**, *34*, 449−530.

(29) Andrade, J. D.; Bo1es, E. S.; Stassen, H. Computational Study of Room Temperature Molten Salts Composed by 1-Alkyl-3-methyl-imidazolium Cations-Force-Field Proposal and Validation. *J. Phys. Chem. B* **2002**, *106*, 13344−13351.

(30) Ghatee, M. H.; Moosavi, F. Physisorption of Hydrophobic and Hydrophilic 1-Alkyl-3-methylimidazolium Ionic Liquids on the Graphenes. *J. Phys. Chem. C* **2011**, *115*, 5626−5636.

(31) Liu, Z. P.; Huang, S. P.; Wang, W. C. A Refined Force Field for Molecular Simulation of Imidazolium-Based Ionic Liquids. *J. Phys. Chem. B* **2004**, *108*, 12978−12989.

(32) Allen, C.; Sambasivarao, S. V.; Acevedo, O. An Ionic Liquid Dependent Mechanism for Base Catalyzed β-Elimination Reactions from QM/MM Simulations. *J. Am. Chem. Soc.* **2013**, *135*, 1065−1072.

(33) Tsuzuki, S.; Tokuda, H.; Hayamizu, K.; Watanabe, M. Magnitude and Directionality of Interaction in Ion Pairs of Ionic

Liquids: Relationship with Ionic Conductivity. *J. Phys. Chem. B* **2005**, *109*, 16474−16481.
(34) Valencia, H.; Kohyama, M.; Tanaka, S.; Matsumoto, H. *Ab initio* study of EMIM-BF_4 molecule adsorption on Li surfaces as a model for ionic liquid/Li interfaces in Li-ion batteries. *Phys. Rev. B* **2008**, *78*, 205402-1−205402-13.
(35) Barnard, A. S.; Xu, H. F. An Environmentally Sensitive Phase Map of Titania Nanocrystals. *ACS Nano* **2008**, *2*, 2237−2242.
(36) Zanella, R.; Giorgio, S.; Henry, C. R.; Louis, C. Alternative Methods for the Preparation of Gold Nanoparticles Supported on TiO_2. *J. Phys. Chem. B* **2002**, *106*, 7634−7642.
(37) Pensado, A. S.; Padua, A. A. H. Solvation and Stabilization of Metallic Nanoparticles in Ionic Liquids. *Angew. Chem., Int. Ed.* **2011**, *50*, 8683−8687.
(38) Steiner, T.; Saenger, W. Geometry of C-H···O hydrogen bonds in carbohydrate crystal structures. Analysis of neutron diffraction data. *J. Am. Chem. Soc.* **1992**, *114*, 10146−10154.
(39) Martins, J. F. M; Ferreira, A. R.; Konstantinova, E.; De Abreu, H. A.; Souza, W. F.; Chiaro, S. S. X.; Dias, L. G.; Leitão, A. A. Interactions between 1-butyl-3-methylimidazolium tetrafluoroborate ionic liquid and γ-Al_2O_3 (100) surface calculated by density functional theory. *Int. J. Quantum Chem.* **2012**, *112*, 3234−3239.
(40) Ninham, B. W. On progress in forces since the DLVO theory. *Adv. Colloid Interface Sci.* **1999**, *83*, 1−17.
(41) Li, Y. F.; Liu, Z. P.; Liu, L. L.; Gao, W. G. Mechanism and Activity of Photocatalytic Oxygen Evolution on Titania Anatase in Aqueous Surroundings. *J. Am. Chem. Soc.* **2010**, *132*, 13008−13015.
(42) Barnard, A. S.; Zapol, P.; Curtiss, L. A. Anatase and rutile surfaces with adsorbates representative of acidic and basic conditions. *Surf. Sci.* **2005**, *582*, 173−188.
(43) Dai, Y. Q.; Cobley, C. M.; Zeng, J.; Sun, Y. M.; Xia, Y. N. Synthesis of Anatase TiO_2 Nanocrystals with Exposed {001} Facets. *Nano Lett.* **2009**, *9*, 2455−2459.